Alloy scattering limitation on the mobility of holes in p-type $GaAs_{1-x}Sb_x$

Cameron Dale[a)]
Department of Physics, Simon Fraser University, Burnaby, BC, V5A 1S6

The hole mobilities in the $GaAs_{1-x}Sb_x$ system is been investigated for $0.0 \leq x \leq 1.0$. Undoped room temperature mobilities are used to examine the scattering as a function of the Sb content. Two scattering mechanisms are considered: ionised impurity and alloy scattering. The alloy scattering potential is found to be 1.868 eV, which is about twice the theoretical value. Samples of various doping levels are also used, from undoped to heavily doped, to examine the temperature dependence of the mobility. The van der Pauw-Hall method is employed to determine the mobility at temperatures ranging from 4.2 K to 320 K. Three scattering mechanisms are considered: ionised impurity, lattice, alloy, and surface charge scattering. Surface charge scattering is found to be negligible, but lattice scattering is important at high temperatures. Ionised impurity scattering is dominant at low temperatures, where two forms for it are found: one for non-degenerate semiconductors, and one for degenerate semiconductors. The alloy scattering potential is determined for each of the samples, and lies in the range of 1.3 to 1.6 eV. This is also larger than the theoretical value. The discrepancies in the alloy scattering potentials may be attributed to not considering deformation potential scattering, which may be significant for these samples.

[a)] Electronic mail: cdale@sfu.ca

I. Introduction

The $GaAs_{1-x}Sb_x$ alloys have recently attracted interest as they are being used in the manufacture of NpN InP/GaAsSb/InP double-heterojunction bipolar transistors (DHBTs). These transistors have several desirable characteristics. The type II staggered conduction and valence band alignments of the devices are beneficial to their performance.[1] The valence band offset in this device is about 760 meV, which is enough to effectively block any hole back injection into the emitter.[2] The HBTs have a very small offset voltage and a low turn-on voltage, which makes them suitable for low voltage, high frequency, and microwave applications. However, a large amount of scattering is limiting the hole mobility in the p-type $GaAs_{1-x}Sb_x$ base to 20-30 cm^2/Vs. This is then creating a large resistance in the base that reduces the maximum oscillation frequency of the transistors. This also imposes a minimum size limit on the base that prevents further reductions. Very little is known about the scattering involved in this relatively new material, especially at the high doping levels that are used in these devices.

This work consists of an investigation of the transport of holes in $GaAs_{1-x}Sb_x$ to try and understand the scattering processes involved in this material. First, data taken for many undoped samples at room temperature is analysed to see if alloy scattering is present, and how strong an effect it has. Then, six samples are tested with Sb contents varying from GaAs (x = 0) to GaSb (x = 1). These samples have various amounts of doping, from undoped to acceptor densities of 10^{20} cm^{-3}. Temperature dependent Hall data is taken using the van der Pauw-Hall method at temperatures ranging from 4.2 K to 300 K. These measurements yield many interesting characteristics of the material, most importantly the mobility. The temperature dependence of the mobilities for these samples is then fit to theoretically proposed models from other papers. These fits give valuable information on the various scattering processes present, and their relative intensities.

II. Theory

A. Semiconductor Band Structure

Semiconductors have a band structure, where transitions between bands occur but require the addition of energy to the system. A typical energy band structure approximation for a direct band gap semiconductor, near the band gap, is shown in Figure 1. The semiconductor is called direct because there is no change required in the wavevector k to go from the valence to the conduction band. Note that there is a gap between the allowed energies of the valence band and those of the conduction band. Also, there is degeneracy in the valence band at the band gap. As is typical for semiconductors, the bands are plotted with electron energy on the y-axis. Since the semiconductors dealt with in this work are all p-type, the energy of

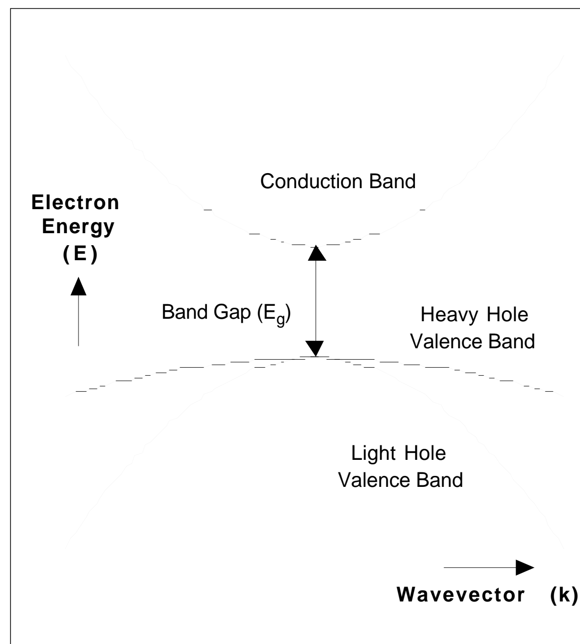

Figure 1: The band structure of a typical direct band gap semiconductor.

their holes will all be the negative of the electron energy. Therefore, the band structure should be turned upside down to get increasing hole energy in the positive y-direction. The conduction band has many holes trying to gain enough energy to make it to one of the valence bands.

In this band structure, the holes near the centre of the valence bands do not act as free charges. This behaviour can be accounted for by using an effective mass for the holes, instead of the mass of a free electron.[3] This mass is given by

$$\frac{1}{m^*} = \frac{1}{\hbar^2}\frac{d^2E(k)}{dk^2}, \tag{1}$$

where $\hbar$ is the constant h/2π and *E(k)* is the energy of the band as a function of the wavevector (this is what was plotted in Figure 1 to get the band structure). The reciprocal of the effective mass is therefore proportional to the curvature of the band, and since the two valence bands have different curvatures, then there will be two effective masses for holes. These are referred to as heavy hole (m_{hh}) and light hole (m_{lh}) masses, and are commonly combined to give an overall effective mass for holes by assuming that the valence bands are ellipsoidal.[4]

$$m_p^* = \left(m_{lh}^{3/2} + m_{hh}^{3/2}\right)^{2/3} \tag{2}$$

B. Degenerate p-type Semiconductors

Degenerate semiconductors are those in which the doping level is so large, that there can be hole transport in the acceptor levels created by the dopant, and not just in the valence band. Normally, a semiconductor is treated as non-degenerate to simplify the equations involved. This is usually true because the doping level is low enough that the few impurity atoms present are so widely spaced that there could not possibly be charge transport between them. This is not the case in most of the samples studied here, as the doping levels are high enough in some to make the semiconductor degenerate. A typical judge of degeneracy is that a semiconductor is said to be degenerate if its Fermi level (E_F) is within $4k_BT$ of the valence band.

Using the Fermi-Dirac distribution

$$f(E) = \frac{1}{e^{(E-E_F)/k_BT}+1}, \tag{3}$$

the density of states in the valence band can be shown to be[5]

$$N_v = 2\left(\frac{2\pi m_p^* k_BT}{h^2}\right)^{3/2}. \tag{4}$$

The concentration of holes in the valence band is then given by[6]

$$p = N_vF_{1/2}(\eta) = N_v\frac{2}{\sqrt{\pi}}\int_0^\infty \frac{x^{1/2}dx}{e^{x-\eta}+1} \tag{5}$$

with the dimensionless variables

$$x = \frac{E_v - E}{k_BT} \quad \text{and} \quad \eta = \frac{E_v - E_F}{k_BT}. \tag{6}$$

In these equations, E_v is the valence band energy, and $F_{1/2}(\eta)$ is the Fermi-Dirac integral of order 1/2. Using the measured concentration of holes in the valence band and the calculated density of states for the valence band, this integral can be solved (using tables[7] or analytically using a program such as Maple) to yield the number of k_BT that the Fermi level is above the valence band.

C. The Hall Effect

The Hall effect is based on the geometry shown in Figure 2. The block shown in the figure is a p-type (in this case) semiconducting bar. A magnetic field is applied in the z-direction, and is perpendicular to an electric field applied as a current in the x-direction. The force on the moving holes due to the magnetic field in the bar gives rise to the Hall effect.

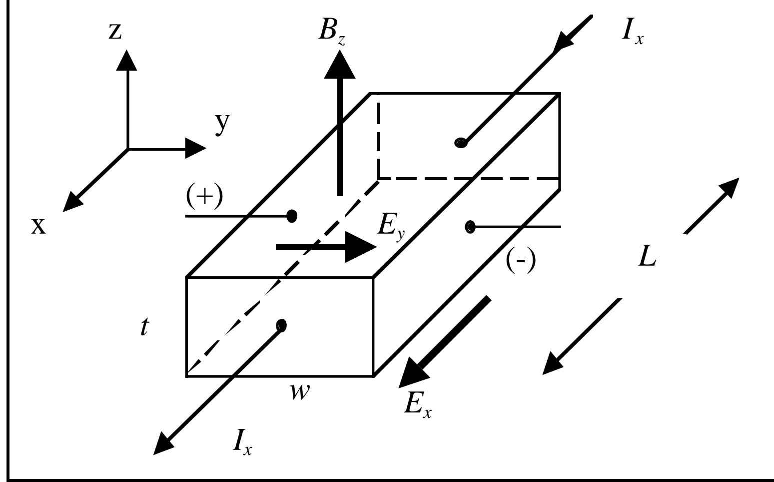

Figure 2: The geometry for the Hall effect.

The Lorentz force law

$$\boldsymbol{F} = q(\boldsymbol{E} + \boldsymbol{v} \times \boldsymbol{B}), \tag{7}$$

can be used to give the force on the holes in the y-direction of Figure 2.

$$F_y = e\left(E_y - v_x B_z\right) \tag{8}$$

In the steady state solution, therefore, the force in the y-direction must be zero, and so an electric field must be set up in the positive y-direction to balance the magnetic force on the moving charges in the negative y-direction. This gives a voltage across the bar of

$$V_y = E_y w = v_x B_z w. \tag{9}$$

The establishment of this electric field is known as the Hall effect, and the resulting voltage in Eq. (9) is called the Hall voltage.

The velocity in the x-direction can be substituted for by the current, using the equation

$$\frac{I_x}{wt} = ep\langle v_x \rangle. \tag{10}$$

This gives an equation for the Hall voltage of

$$V_y = \frac{I_x}{epwt} B_z w = \left(\frac{1}{ep}\right)\frac{I_x B_z}{t} = R_H \frac{I_x B_z}{t}, \tag{11}$$

where R_H is the Hall coefficient. Therefore, a measurement of the Hall voltage for a known current and magnetic field will give the hole concentration and the Hall coefficient

$$p = \frac{I_x B_z}{eV_y t} \qquad R_H = \frac{1}{ep}. \tag{12}$$

From a measure of the voltage across the bar V_x while the current I_x is on, and knowledge of the dimensions of the bar, the resistivity can be determined

$$\rho = \frac{Rwt}{L} = \frac{V_x wt}{I_x L}. \tag{13}$$

Since the conductivity is related to the resistivity and to the mobility, then the Hall mobility can be determined from the resistivity

$$\mu_H = \frac{\sigma}{ep} = \frac{1/\rho}{1/R_H} = \frac{R_H}{\rho}. \tag{14}$$

The mobility calculated from Eq. (14) has been labelled μ_H and called the Hall mobility to differentiate it from the drift or conductivity mobility. The actual drift mobility of a sample will differ from the Hall mobility by the effective Hall factor

$$\mu_H = r_{eff}\mu . \qquad (15)$$

The effective Hall factor, r_{eff}, will in general depend on temperature and composition of the sample, and would have to be taken into account to get accurate results. The Hall factor can normally be taken to be about 1, although this is not quite accurate. However, it turns out that that the effective Hall factor is 1 for degenerate semiconductors. Most of the samples considered here are degenerate, so the Hall factor will not be used, and μ will be used to indicate the Hall and drift mobilities.

D. van der Pauw-Hall Method

There is a serious problem with determining the mobility of semiconductors from the Hall effect described in the previous section. According to Figure 2, the sample must be in the shape of a bar, with samples on four of the six sides. This presents an insurmountable problem for most samples, as they are grown as a thin layer on top of a substrate, and only have one side that is accessible to make contacts on. Luckily, a method has been developed for measuring the resistivity and mobility of samples of an arbitrary shape. This method is known as the van der Pauw-Hall method,[8] and a brief summary of its derivation will be considered here.

The geometry for the van der Pauw-Hall method is shown in Figure 3. It is a flat sample of arbitrary shape with four contacts fixed on arbitrary places along the circumference. The derivation relies on four conditions being fulfilled: the contacts are at the circumference of the sample, the contacts are sufficiently small, the sample is homogeneous in thickness, and the surface of the sample is singly connected.

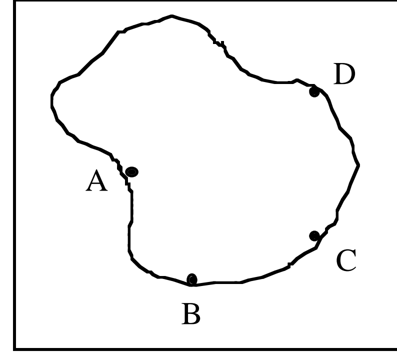

Figure 3: The geometry for the van der Pauw-Hall effect.

The resistance $R_{AB,CD}$ is defined as the potential difference between D and C, when there is unit current flowing from A to B. The corresponding resistance, $R_{BC,DA}$, is similarly defined.

$$R_{AB,CD} = \frac{V_D - V_C}{I_{AB}} \qquad R_{BC,DA} = \frac{V_A - V_D}{I_{BC}} \qquad (16)$$

It will not be proven here, but it can be shown[8] that

$$e^{-\pi R_{AB,CD} d/\rho} + e^{-\pi R_{BC,DA} d/\rho} = 1, \qquad (17)$$

where d is the thickness of the sample. Assuming that $R_{AB,CD}$ and $R_{BC,DA}$ are almost equal, this can be rearranged to give a resistivity of

$$\rho = \frac{\pi d}{\ln 2}\left(\frac{R_{AB,CD} + R_{BC,DA}}{2}\right). \qquad (18)$$

This equation can be improved by replacing the average over two of the resistances, with the average over all four of them.

If a magnetic field B is then applied perpendicular to the surface of the sample, the resistance $R_{BD,AC}$ will change to $R'_{BD,AC}$ as the potential difference changes from $V_A - V_C$ to $V'_A - V'_C$. This was not discussed in the previous section, because no field being applied

means that V_y was originally zero, due to the symmetry of the bar. In this case, there is no symmetry, and so there is a measurable voltage without the field, and the Hall voltage would then be defined as the change in voltage from the no field case. The Hall coefficient will be given by

$$R_H = \frac{d}{B}\frac{\Delta(V_A - V_C)}{I_{BD}} = \frac{d}{B}\left(\frac{(V_A' - V_C')}{I_{BD}} - \frac{(V_A - V_C)}{I_{BD}}\right) = \frac{d}{B}\left(R_{BD,AC}' - R_{BD,AC}\right). \qquad (19)$$

The Hall mobility is then given by

$$\mu_H = \frac{R_H}{\rho} = \frac{d}{B}\left(\frac{R_{BD,AC}' - R_{BD,AC}}{\rho}\right) = \frac{2\ln 2}{\pi B}\left(\frac{R_{BD,AC}' - R_{BD,AC}}{R_{AB,CD} + R_{BC,DA}}\right), \qquad (20)$$

which is independent of the thickness of the sample and any other dimensions. This equation can also be improved by replacing the change in resistance for one set of corners, with the average of the change in resistance for both sets of corners.

E. Scattering Processes

The main focus of this work is the alloy scattering present in the samples. Therfore, it will be described in detail, and an equation will be given to describe it's effect. However, the other scattering processes present will not be explained in much detail, nor will exact equations be used. It will suffice to explain the origin of the scattering, and to give a temperature dependence for it. The temperature dependence of these other scattering processes is necessary to accurately account for the alloy scattering effect on the mobility of the sample. All of these effects on the mobility of holes in the samples can be taken into account by using Mathiesen's rule[9]

$$\frac{1}{\mu} = \frac{1}{\mu_1} + \frac{1}{\mu_2} + \frac{1}{\mu_3} + \ldots. \qquad (21)$$

This equation relates the total mobility of a sample to the mobilities due to the various types of scattering. Because of the reciprocal form of the equation, the scattering mechanism with the lowest mobility will dominate.

1. Alloy Scattering

This type of scattering comes about in alloys, where a hole could be in a potential created by one type of atom, and then enter into a potential created by another type of atom. The simplest way to think about alloy scattering is as if the hole was approaching a quantum well, as shown in Figure 4. Quantum mechanics shows that there is a finite possibility that the hole will be reflected back from the quantum well. In 3-dimensions, the hole would have a finite possibility of being scattered from its original path. It would be expected that the probability of being scattered would depend somehow on the depth of the quantum well.

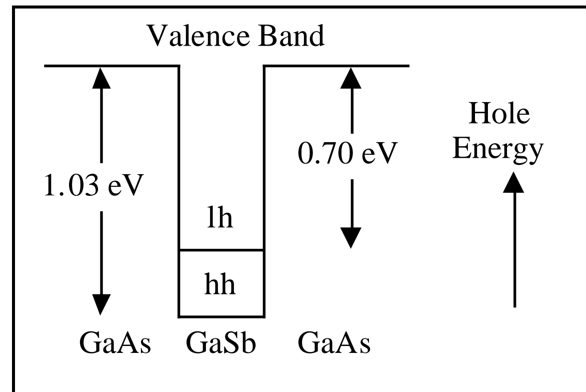

Figure 4: The valence band offset in the band structure of a GaAsSb alloy.

To be more quantitative, a commonly used scattering rate for charges in an alloy has been derived.[10] The alloy needs to be a ternary III-V compound where one of the elements is common to both of the constituent compounds. Therefore, $GaAs_{1-x}Sb_x$ qualifies since it is an alloyed combination of GaAs and GaSb. To derive the formula for alloy scattering,

the zinc blende structure of the alloy is recognised to be a combination of two interpenetrating fcc lattices, one of all Ga atoms and the other with both As and Sb atoms. The actual crystal is then thought of as divided into two parts. The virtual crystal is a perfectly periodic array of composition-weighted potentials due to the different kinds of atoms making up the crystal. There is also a random part present due to the difference between the actual crystal potential and the virtual crystal potential at a given lattice point.

This virtual crystal concept can be used to simplify the evaluation of the integrals involved. For a completely random alloy, the square of the transition matrix between initial and final states is

$$|M(\boldsymbol{k},\boldsymbol{k'})|^2 = \frac{x(1-x)}{N\Omega^2}\left|\int_{\infty\, volume} \psi_{k'}^{*}\Delta U(r)\psi_k d\mathbf{r}\right|^2 . \quad (22)$$

The potential $\Delta U(r)$ in this equation will be assumed to be a square well potential, with a range given by r_o.

$$\Delta U(r) = \begin{Bmatrix} \Delta E & r \le r_o \\ 0 & r > r_o \end{Bmatrix} \quad (23)$$

The integral can now be evaluated for the range of the square well potential only

$$|M(\boldsymbol{k},\boldsymbol{k'})|^2 = \frac{x(1-x)}{N\Omega^2}\left|\int_0^{r_o} e^{-i\Delta\boldsymbol{k}\bullet\boldsymbol{r}}(\Delta E)r^2 dr\sin\theta\, d\theta\, d\phi\right|^2 . \quad (24)$$

Taking θ as the angle between $\Delta\boldsymbol{k}$ and $\boldsymbol{k}$' gives

$$\begin{aligned} |M(\boldsymbol{k},\boldsymbol{k'})|^2 &= \frac{x(1-x)}{N\Omega^2}\left|4\pi\frac{\Delta E}{\Delta k}\int_0^{r_o}\sin(\Delta k r) r dr\right|^2 \\ &= \frac{x(1-x)}{N\Omega^2}\left|4\pi\frac{\Delta E}{(\Delta k)^3}\left(\sin\Delta k r_o - \Delta k r_o\cos\Delta k r_o\right)\right|^2 . \end{aligned} \quad (25)$$

Since the maximum value of $\Delta k r_o$ is much less than 1, the following approximations can be used.

$$\begin{gathered} \sin x \approx x - x^3/6 \qquad x\cos x \approx x - x^3/2 \\ \sin x - x\cos x \approx x^3/3 \end{gathered} \quad (26)$$

Using these approximations gives a final value for the square of the transition matrix of

$$|M(\boldsymbol{k},\boldsymbol{k'})|^2 = \frac{x(1-x)}{N\Omega^2}\left|4\pi\frac{\Delta E}{(\Delta k)^3}\frac{(\Delta k r_o)^3}{3}\right|^2 = \left(\frac{4\pi r_o^3}{3\Omega}\right)^2\frac{x(1-x)}{N}(\Delta E)^2 . \quad (27)$$

The choice of the length of the square well potential interaction is rather arbitrary, but a good choice would be to use the nearest neighbours distance to approximate it. For a zinc blende lattice, the nearest neighbour distance is

$$r_o = \frac{1}{4}\sqrt{3}a , \quad (28)$$

where a is the lattice parameter. Putting this equation into the transition matrix gives

$$|M(\boldsymbol{k},\boldsymbol{k'})|^2 = \left(\frac{3a^3}{4\Omega}\right)^2\frac{3\pi^2}{16}\frac{x(1-x)}{N}(\Delta E)^2 = \frac{3\pi^2}{16}\frac{x(1-x)}{N}(\Delta E)^2 . \quad (29)$$

This expression for the transition matrix can now be used in the Boltzmann transport equation to get an expression for the scattering rate. This involves the use of the common

relaxation time approximation. Evaluating the collision integral term for the Boltzmann transport equation

$$\frac{1}{\tau(\varepsilon)} = \frac{V}{8\pi^2}\int \frac{2\pi}{\hbar}\left|M(\boldsymbol{k},\boldsymbol{k}')\right|^2 \delta\left(\varepsilon_k - \varepsilon_{k'}\right)d\boldsymbol{k}' \tag{30}$$

gives the relaxation time expression as a function of energy, ε

$$\tau(\varepsilon) = \frac{8N_A\hbar^4\varepsilon^{-1/2}}{3\sqrt{2}\pi\, x(1-x)(\Delta E)^2\left(m^*\right)^{3/2}(k_BT)^{1/2}}. \tag{31}$$

This can be converted into a mobility

$$\begin{aligned}\mu_{AL} &= \frac{e\langle\tau\rangle}{m^*} = \frac{e}{m^*}\frac{\int_0^\infty \varepsilon^{3/2}\tau(\varepsilon)e^{-\varepsilon/k_BT}d\varepsilon}{\int_0^\infty \varepsilon^{3/2}e^{-\varepsilon/k_BT}d\varepsilon} \\ &= \frac{32\sqrt{2}}{9\pi^{3/2}}\frac{e\hbar^4}{v_a x(1-x)(\Delta E)^2\left(m^*\right)^{5/2}\left(k_BT\right)^{1/2}}\end{aligned}, \tag{32}$$

where $v_a = 2/N$ is a measure of the density of the sample. This equation shows the standard temperature dependence of $T^{-0.5}$ for alloy scattering.

An expected value for the alloy scattering potential, ΔE, can thus be determined. As this is the height of the quantum well encountered by the holes, it makes sense to use the valence band offset as an estimate for the potential. Therefore, for $GaAs_{1-x}Sb_x$ the alloy scattering potential is predicted to be on the order of 1 eV.

2. *Impurity Scattering*

Impurity scattering is a form of defect scattering, as is alloy scattering. It arises from the holes in the sample being scattered off of impurities in the lattice. These impurities can be unwanted atoms that found their way into the sample, but this is rare and so their concentration is small. Most impurities in the sample are due to dopants that were added to the sample on purpose to increase the number of carriers. These dopants can be neutral or ionised, with the ionised ones having a stronger scattering effect due to their charge. Since the impurities are almost all ionised in degenerately doped semiconductors, only ionised impurity scattering is considered here. The ionised impurity scattering of holes has been shown[11] to depend on temperature as

$$\mu_{II} \propto T^{1.5}. \tag{33}$$

This equation shows that ionised impurity scattering will dominate at low temperatures, but will be negligible at high temperatures.

The preceding argument and Eq. (33) show that as the temperature goes to zero, so does the mobility. This is not the case, however, for degenerately doped semiconductors. In non-degenerate semiconductors, as the temperature drops to zero so does the number of holes, as they do not have enough thermal energy to ionise. This reduces the mobility to zero at low temperatures. In the case of degenerate semiconductors, the holes do not need to ionise as they can move freely in the band formed by the acceptor dopants. Therefore, the mobility of degenerate semiconductors will peak at very low temperatures.

In order to represent this factor in the fit, Eq. (33) will have to be modified. If it is not, then ionised impurity scattering would dominate at low temperatures and cause the theoretical mobility to go to zero, rather than a constant value. One option is to not include ionised impurity scattering in the calculation for degenerately doped semiconductors, and

instead use a constant mobility that does not depend on temperature. However, this will not be useful for intermediary cases where the sample is on the border between degenerate and non-degenerate doping. Also, because this constant mobility will also have a constant value at high temperatures, this will strongly affect the high temperature region of the theoretical mobility, where ionised impurity scattering is not expected to have any effect.

The solution opted for here is to combine the two cases into a single ionised impurity mobility, using two unknown constants. This has the form

$$\mu_{II} = C + AT^{1.5}, \tag{34}$$

where C is the constant mobility that will be approached as the temperature goes to zero and A is the proportionality factor for the ionised impurity scattering. This will then provide the proper low temperature behaviour of approaching a constant value, and will not affect the high temperature behaviour as the ionised impurity scattering will take off.

3. Lattice Scattering

Lattice scattering is any scattering process that comes about because of the existence of the lattice. The nuclei in this periodic arrangement vibrate around their central position. This scattering therefore involves phonons or variations of the potential from one lattice point to another. This includes acoustic and optical deformation potential scattering, and acoustic and optical polar scattering. The lattice scattering of holes has been shown[11] to depend on temperature as

$$\mu_{LA} \propto T^{-2.3}. \tag{35}$$

This equation shows that lattice scattering will have almost no effect at low temperatures, but will have a large effect at high temperatures.

4. Deformation Potential Scattering

One type of lattice scattering is not covered by Eq. (35): deformation potential scattering. This scattering mechanism will occur due to the strain of a lattice mismatch between the two materials of the alloy. It has not been included in the derivation of Eq. (35) because the derivation was done for the more common $Al_{1-x}Ga_xAs$ alloys, in which the two constituents are almost lattice matched. GaAs has a lattice constant of 5.65 Angstroms, while GaSb’s lattice constant is 6.06 Angstroms. This 0.41 Angstrom difference may not seem like much, but it is much larger than the 0.01 Angstrom difference found in the AlAs/GaAs system. Therefore, this scattering is similar to what is found in $Si_{1-x}Ge_x$ alloys, which are strained due to their lattice mismatch. Deformation potential scattering can be shown[12] to have a temperature dependence of

$$\mu_{DP} \propto T^{-0.5}. \tag{36}$$

This scattering mechanism has the same temperature dependence as alloy scattering, and will therefore be almost indistinguishable from it.

5. Space Charge Scattering

Space charge scattering occurs as a result of charge carriers interacting with other carriers. This scattering mechanism can be shown[12] to have a temperature dependence of

$$\mu_{SC} \propto T^{-0.5}. \tag{37}$$

This temperature dependence is also the same as for alloy scattering and deformation potential scattering, so it is difficult to differentiate between these three.

III. Experiment

A. Sample Preparation

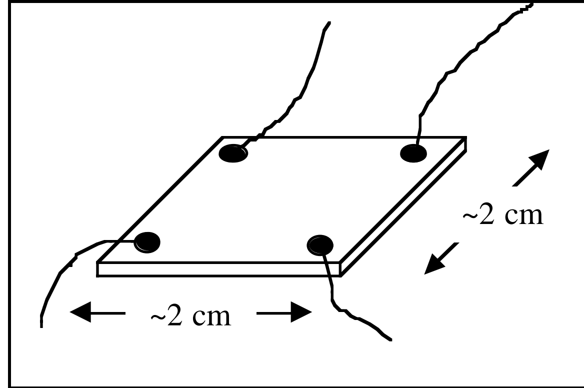

Figure 5: An example of a Hall sample.

All of the $GaAs_{1-x}Sb_x$ samples for this experiment were grown by metalorganic vapour phase epitaxy (MOVPE) on InP (001) oriented substrates. The details of the growth are described elsewhere.[2] The sample is then cleaved into an appropriate size, and contacts are attached. The Sn contacts used are connected by placing small bits of Sn (with the outer oxide layer removed by acid) on the appropriate location of the sample. The sample is the heated up to 350° in an oxygen-free environment, at which point the Sn melts and forms a contact with the surface of the semiconductor. The sample is then cooled, and small wires are attached to the contacts with a soldering iron. An example of the approximate size and location of the contacts on a finished sample is shown in Figure 5.

B. Liquid Helium Cryostat

The temperatures required for this work are in the range of 4.2 K to room temperature; therefore, a liquid helium cryostat is necessary. The "Super Varitemp" system that was used to obtain these temperatures is shown in Figure 6. The apparatus consists of three concentric cylinders. The outer cylinder is a liquid nitrogen reservoir that keeps the entire apparatus cold. Inside of that is the liquid helium reservoir, where the liquid helium is stored for use in the cooling of the sample. There is a superconducting rod used as a level sensor, which is connected to an American Magnetics 110A Liquid Helium Level Meter to measure the level of liquid helium in the reservoir. Within that reservoir is the sample chamber. Each cylinder is separated from the others, and from the outside, by vacuum jackets continuously pumped on by a diffusion pump and a mechanical vacuum pump.

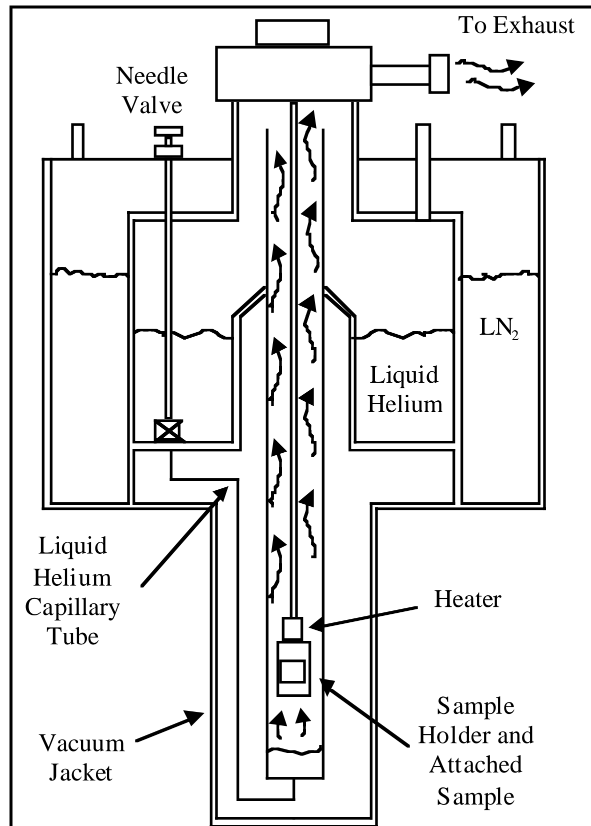

Figure 6: A cross-section of the "Super Varitemp" liquid helium cryostat.

The temperature of the sample is controlled by two counterproductive sources. The needle valve at the top of the cryostat opens a small capillary tube from the liquid helium reservoir to the bottom of the sample tube. The liquid helium can be pulled down through this by gravity, or the liquid helium reservoir can be pressurised so that the liquid helium is pushed through the tube. This allows for flow control of the liquid helium into the bottom of the sample chamber. There is also a heater and temperature sensor on the sample holder, which are both connected

to a LakeShore DRC-91CA Controller. This controller has a temperature setting on it, and it reads the temperature of the sample and adjusts the output to the heater accordingly. If the needle valve is set properly to an appropriate flow rate, then the only adjustments that need to be made will be on the temperature controller to get a full range of 4.2 K to 320 K.

C. Electronics

There are three electronic devices involved in the electrical connections to the sample. The first is a Keithley 220 Programmable Current Source, which supplies the currents required for the Hall effect measurements. The Hall voltages are measured using a Keithley 182 Sensitive Digital Voltmeter. The final device is a Keithley 706 Scanner, which allows switching between the different connections on the sample. The four wires from the sample go into the scanner, and the current source and digital voltmeter are also connected to it. The scanner can be programmed to connect either device to any two of the contacts on the sample.

There are also four electronic devices involved in the production of the magnetic field for the Hall measurements. The bottom of the sample chamber is inserted into a Bruker B-M6 Magnet. The current for the magnet is provided by a Bruker B-MN 90/30 C5 Current Source. Reversing this current using the BRUKER B-U5 Reverser will reverse the direction of the magnetic field. The BRUKER B-H15 Field Controller controls the current source and reverser, and also has a Hall sensor connected to it to measure the field in the magnet. The desired field can be set on the controller, and it will adjust the current and reverser appropriately to create the magnetic field.

D. Computer Control

A computer in the laboratory controls all of the devices mentioned in the Electronics section above. Each device is connected to the computer’s IEEE488 bus by GPIB cables, which allows for control of the devices and for reading values from them. The entire Hall measurement has been automated in a single Visual Basic (for Windows) program. This program is used for the setting of the magnetic field strength, the current, the amount of time for the voltmeter to integrate for, and the thickness of the sample. The magnetic field strength was kept constant at 5000 Gauss (0.5 Tesla) for all the samples. This is a large field, but it was necessary due to the small mobilities of the samples. The current varied from 10^{-4} to 10^{-6} Amps from sample to sample, as some had a larger resistivity than others did. The larger currents are better for reducing noise, but the resistivity of some of the samples was so high that the current had to be turned down so that the voltages obtained were not too large. The thickness of the samples varied from 0.06 to 3 microns.

This program, once begun, will take all the necessary measurements while changing all the necessary controls, and then use the measurements to calculate all the relevant data. The first measurements are taken without the magnetic field, and are used to calculate the resistivity. The set current is supplied to two neighbouring contacts, and the voltage at the other two contacts is measured. The current is then reversed and the voltage is measured again. The absolute values of these two voltages is then averaged, to remove any unwanted offsets in the measurements. This is then repeated for each of the four pairs of neighbouring contacts, and the four values obtained are averaged to obtain an average overall voltage. This average value is then used in Eq. (18) to obtain the resistivity of the sample.

Next, the magnetic field is turned on and more measurements are taken. This time, the measurements are done on pairs of contacts that are not neighbours, but are instead

located in opposite corners. The set current is supplied between two contacts in opposite corners and the voltage difference is measured between the other two contacts. This is done for positive and negative current, and then the average of the absolute value is used. The measurement is then repeated for the other pairs of contacts. The field is then reversed and the 4 measurements are repeated. The measurements for one pair of contacts, for both the positive and negative fields, are combined to get the average change in resistance from the zero field case. This is then combined with the average change in resistance for the other pair of contacts, and these are averaged and used in Eq. (19) to calculate the Hall coefficient. Eq. (20) is then used with this Hall coefficient and the resistivity from the first measurements to give the mobility of the sample. The Hall coefficient is also used to calculate the bulk concentration of holes in the semiconductor, using Eq. (12).

E. Samples

Six samples were analysed using the method outlined above. They varied in content from pure GaAs to pure GaSb, and ranged in hole concentration from undoped to heavily doped. The values for the hole concentration and content are shown in Figure 7. Note that the undoped sample is included in this graph at a hole concentration of 10^{16} cm^{-3}, which is the average bulk hole concentration determined from the Hall measurements.

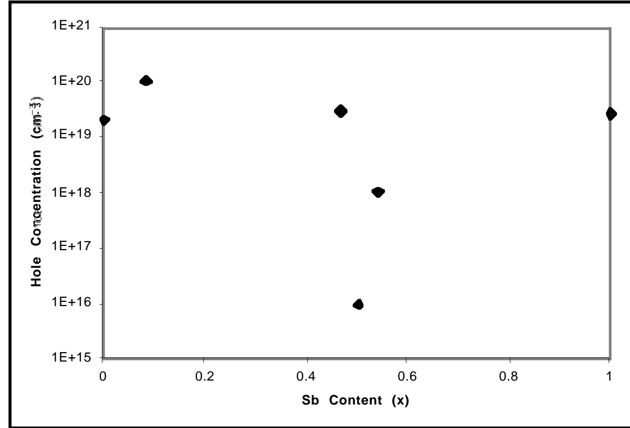

Figure 7: The hole concentrations and Sb content for the six samples that were analysed.

IV. Analysis

A. Room Temperature Alloy Scattering

The first data obtained for this experiment was not from the temperature dependent Hall measurements described above. Instead, Hall mobilities at room temperature that had been previously measured for samples ranging in Sb content were gathered. These mobilities are plotted in Figure 8, along with the fit done to them. The fit involved two types of scattering: ionised impurity and alloy scattering. The alloy scattering mobility of Eq. (32) has been used, with the alloy scattering potential being allowed to vary in the fit. For the Sb content dependence of ionised impurity scattering, an approximate form has been used[13] where the mobility is proportional to $m_p^{*\,-0.5}$, where m_p^* is the effective hole mass and therefore depends

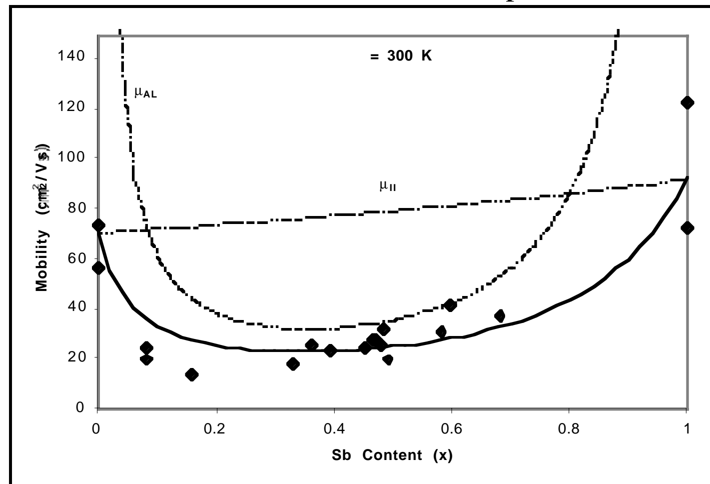

Figure 8: The room temperature mobility of samples with varying Sb content. The dashed lines are individual scattering mobilities and the solid line is the total mobility fit to the experimental data.

on the content. However, Figure 8 shows that this leads to almost no dependence of ionised impurity scattering on the Sb content, as the ionised impurity mobility is almost linear between GaAs and GaSb.

The fit done to this data is shown in Figure 8. The mobility due to ionised impurity scattering is almost linear with Sb content, whereas the mobility due to alloy scattering is deeply bowed in the middle, and goes to infinity at either end (though not symmetrically). These mobilities have been combined, using Eq. (21), to give the total mobility shown in the figure. This has been fit to the experimental data to yield the fitting parameter, the alloy scattering potential, which has a value of 1.868 eV for the fit shown.

B. Temperature Dependent Scattering

For each of the six samples, mobilities as a function of temperature have been obtained. It only remains to fit this data to the various scattering mechanisms described in the theory. The equation used in fits to the data is as shown in Eq. (32), where the alloy scattering potential ΔE is allowed to vary. The equations for the other scattering processes are summarised below. These equations are derived from Eqs. (34) to (37).

$$\begin{aligned}\mu_{II} &= A_{II}(T/300)^{1.5} + C \\ \mu_{LA} &= A_{LA}(T/300)^{-2.3} \\ \mu_{SC} &= A_{SC}(T/300)^{-0.5}\end{aligned} \tag{38}$$

The deformation potential scattering has not been included, as it has the same temperature dependence as the space charge scattering. Therefore, they are almost indistinguishable, and so only one is needed. In Eq. (38), the three proportionality constants (A_{II}, A_{LA}. and A_{SC}) are allowed to vary, as is the ionised impurity constant (C). The temperature is divided by 300 so that the proportionality constants are in units of mobility (cm^2/Vs), and so that they will be comparable, as they are then the room temperature mobilities of the various scattering mechanisms.

Before any fitting can be done, some values need to be calculated for each sample. These values have been included in Table 1, which also contains the values of the variable parameters obtained from the fitting. The first two rows in the table are the Sb content and acceptor dopant concentrations of the samples. These values are determined when the samples are grown.

The next eight rows of Table 1 are various values that depend on the Sb content of the sample. They are the band gap (E_g), the lattice constant (a), the effective electron mass (m_n*), the light hole effective mass (divided by the mass of a free electron) (m_{lh}*/m_o), the heavy hole effective mass (m_{hh}*/m_o), the effective hole mass (m_p*), the relative dielectric constant (ε_r), and the density (N). Each of these has been calculated by using the known values for GaAs and GaSb, and then assuming that they behave linearly as a function of the Sb content (x).[14,15]

The next row in Table 1 is the bulk concentration of holes (p). Recall that the bulk concentration of holes can be calculated for each measurement taken, using Eq. (12). In general, this concentration will depend on the temperature. However, we find here that it is almost constant over the range of temperatures used. A plot of the bulk concentration of holes as a function of temperature is shown in Figure 9. The one that varies the most is the undoped sample, but even that variance is only about a factor of five. Therefore, the bulk

concentration of holes is considered constant, and is taken to be the average over the entire temperature range. This average is the value shown in Table 1.

The next three rows in the table are the radii (r) of possible hole orbits in the sample for three different methods. The first radius (r_B) is the Bohr radius of orbit, calculated using the hole effective mass m_p* of the sample. The next two radii are calculated from the acceptor doping level of the sample. They are the calculated radii that are available to each ionised acceptor atom, based on the density of acceptors in the sample. The first (r_s) is calculated as if each acceptor were centred in a sphere of radius r_s. The second (r_c) is calculated as if each were centred in a cube of side length $2r_c$ (and therefore a radius of r).

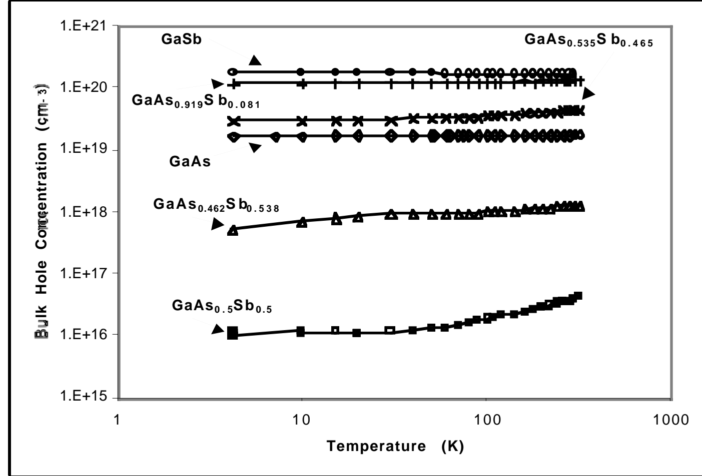

Figure 9: The temperature dependence of the bulk concentration of holes in the six samples.

The next two rows in Table 1 are the values obtained from some simple fits done on the high temperature region of the data. At high temperatures, all of the samples had reached a linear or nearly linear slope on a log-log plot of the mobility as a function of temperature. The fit values were obtained by doing a linear least-squares fitting on the log of the data in this linear region. The first value (T exponent), is the exponent of T that describes the dependence of the mobility on temperature for this linear region. The second value (Δ(T exp)) is the error in the exponent on T in the temperature dependence of the mobility.

Table 1: The values used in the analysis and fitting of the temperature dependent Hall data. The values obtained for the fitting parameters are also included.

Samples	GaAs	$GaAs_{0.919}Sb_{0.081}$	$GaAs_{0.535}Sb_{0.465}$	$GaAs_{0.5}Sb_{0.5}$	$GaAs_{0.462}Sb_{0.538}$	GaSb
x	0.000	0.081	0.465	0.500	0.538	1.000
N_a (cm^{-3})	2.17E+19	1.10E+20	3.14E+19	0.00E+00	1.05E+18	2.80E+19
E_g (eV)	1.423	1.364	1.087	1.062	1.034	0.700
a (Ang)	5.653	5.689	5.859	5.875	5.891	6.096
m_n* (kg)	6.10E-32	1.08E-31	3.29E-31	3.49E-31	3.71E-31	6.38E-31
m_{lh}* / m_o	0.087	0.084	0.070	0.069	0.067	0.050
m_{hh}* / m_o	0.475	0.459	0.384	0.378	0.370	0.280
m_p* (kg)	4.55E-31	4.40E-31	3.68E-31	3.61E-31	3.54E-31	2.68E-31
ε_r	13.20	13.40	14.36	14.45	14.55	15.70
N (cm^{-3})	4.43E+22	4.45E+22	4.54E+22	4.55E+22	4.56E+22	4.68E+22
p (cm^{3})	1.75E+19	1.25E+20	3.68E+19	2.45E+16	1.04E+18	1.71E+20
r_B (Ang)	13.98	14.68	18.81	19.27	19.78	28.25
r_s (Ang)	22.24	12.95	19.66		61.03	20.43
r_c (Ang)	17.93	10.44	15.85		49.19	16.47
T exponent	-0.618	-0.340	-0.474	-0.800	-0.802	-0.393
Δ(T exp)	0.022	0.017	0.007	0.009	0.009	0.011
A_{LA} (cm^2/Vs)	253.510	81.743	81.782	92.404	219.651	394.923
C (cm^2/Vs)	102.122	27.332	48.731	0.000	106.031	146.560
A_{II} (cm^2/Vs)	0.059	0.000	0.000	6399.083	2876.230	0.000
A_{SC} (cm^2/Vs)	958.047					2200.000
ΔE (eV)		1.606	1.292	1.458	1.307	
Scattering	LA+II+SC	LA+II+AL	LA+II+AL	LA+II+AL	LA+II+AL	LA+II+SC

The next five rows are the values obtained from the fit of the scattering mechanisms in Eq. (38) to the temperature dependent Hall data. The first row is the values of the lattice scattering constant (A_{LA}). The second and third rows hold the values of the ionised impurity additive constant (C), and the proportionality constant (A_{II}). The third row has the values of the space charge scattering constant (A_{SC}). The fifth row has the values of the alloy scattering potential (ΔE) used in Eq. (32). The last row in the table (Scattering) contains the type of scattering mechanisms included in the fit.

1. GaAs

This sample is a pure GaAs sample (no Sb) that has been doped to a level of 2.17×10^{19} cm^{-3}. The value for the measured average bulk concentration of holes in this sample, 1.75×10^{19} cm^{-3}, is very close to this doping level. This doping level gives an effective acceptor radius that is almost equal to the Bohr radius. Therefore, this sample is expected to be degenerate. This can be confirmed by calculating the location of the Fermi level, using the bulk concentration of holes and Eqs. (5) and (6). This calculation shows that the Fermi level ranges from being $1.2k_BT$ below the valence band at room temperature, to $10k_BT$ below at 50 K. Therefore, this sample is expected to be completely degenerate.

The temperature dependent Hall data taken for this sample is shown in Figure 10. The scattering parameter for this sample in Table 1 shows that this mobility curve was fit with lattice scattering, ionised impurity scattering, and space charge scattering. Alloy scattering was not used as this is not an alloy.

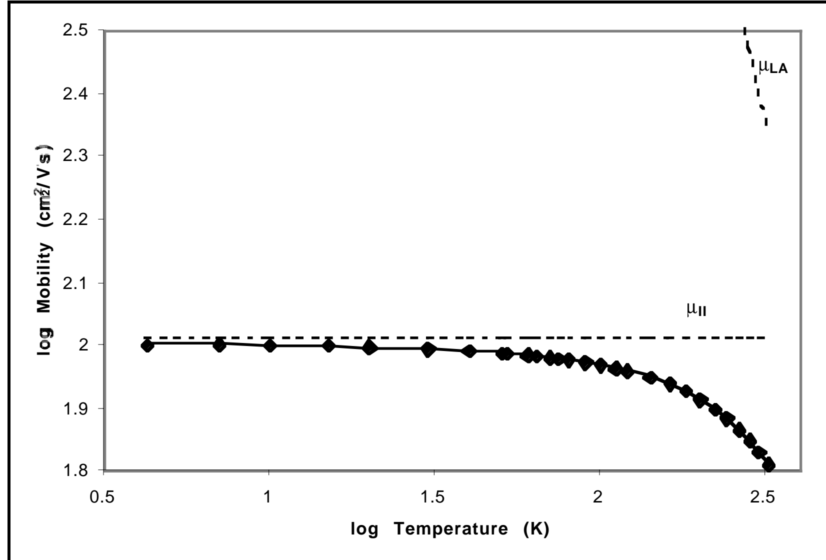

Figure 10: The temperature dependent Hall data for GaAs. The dashed lines are the individual mobilities, while the solid line is the total fit.

The values of the fitting parameters show that the most important scattering mechanism here is the constant in ionised impurity scattering. This can be seen by the small value of the constant, and the almost negligible proportionality factor for ionised impurity scattering. This fact is also clear from Figure 10, as the ionised impurity mobility curve is almost perfectly constant, and is just about the only visible mobility curve on the graph. Lattice scattering is weak, though it does start to have an effect at the highest temperatures, and causes the drop in the experimental mobility. Space charge scattering is almost negligible, as its effect is 4 times weaker than that of lattice scattering.

2. $GaAs_{0.919}Sb_{0.081}$

This sample is an alloy: a mixture of mostly GaAs, and some GaSb. It has been doped to a level of 1.10×10^{19} cm^{-3}, and the value for the average bulk concentration of holes in this sample is 1.25×10^{20} cm^{-3}. This doping level gives an effective acceptor radius

that is smaller than the Bohr radius, so it is expected that the sample will be degenerate. This is confirmed by the location of the room temperature Fermi energy, $7k_BT$ below the top of the valence band. The distance between the two increases as the temperature is lowered, and the Fermi level is buried more and more in the valence bands. Therefore, this sample is expected to be completely degenerate.

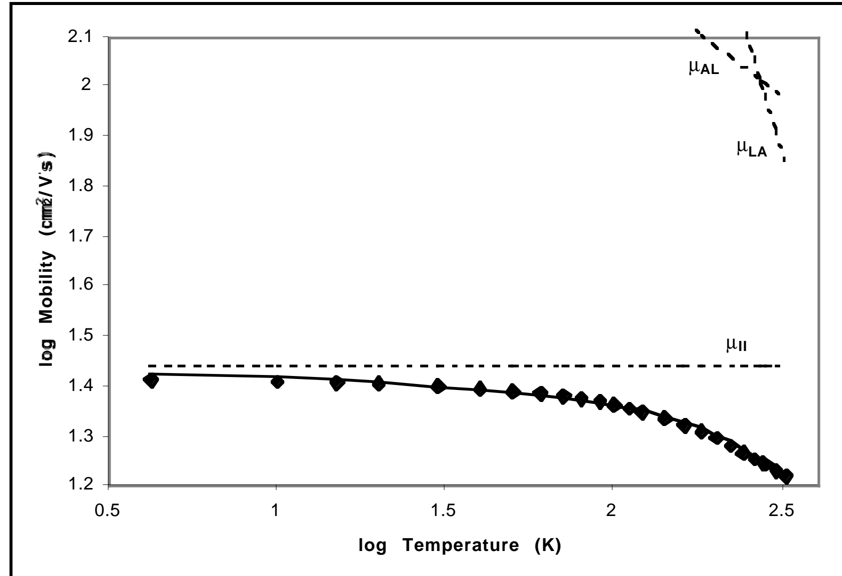

Figure 11: The temperature dependent Hall data for $GaAs_{0.919}Sb_{0.081}$. The dashed lines are the individual mobilities, while the solid line is the total fit.

The temperature dependent Hall data taken for this sample is shown in Figure 11. The scattering parameter for this sample in Table 1 shows that this mobility curve was fit with lattice scattering, ionised impurity scattering, and alloy scattering.

Looking at the graph of the data and the fit, it is obvious that the most important scattering mechanism here is also the constant from the ionised impurity scattering. This can be seen by the small value of the constant, and the zero proportionality factor for ionised impurity scattering in Table 1. In Figure 11, the ionised impurity mobility curve is perfectly constant, and again is almost the only visible mobility curve on the graph. Lattice scattering is weaker than in the GaAs, as its proportionality factor is about three times the constant (compared with about 2.5 times the constant for GaAs). The alloy scattering starts to have an effect at medium high temperatures, where it's stronger than lattice scattering. However, at high temperatures the lattice scattering gets stronger and dominates it.

3. $GaAs_{0.535}Sb_{0.465}$

This sample is an alloy: approximately half is GaAs and half is GaSb. It has been doped to a level of 3.14×10^{19} cm^{-3}, which is very close to the measured average bulk concentration of holes in this sample of 3.68×10^{19} cm^{-3}. This doping level gives an effective acceptor radius that is approximately equal to or smaller than the Bohr

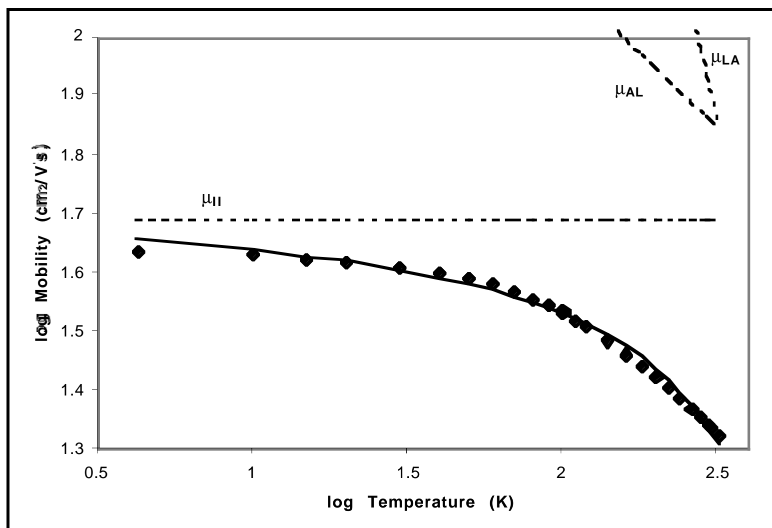

Figure 12: The temperature dependent Hall data for $GaAs_{0.535}Sb_{0.465}$. The dashed lines are the individual mobilities, while the solid line is the total fit.

radius, so it is expected that the sample will be degenerate. This is confirmed by the location of the room temperature Fermi energy $4k_BT$ below the top of the valence band. The distance between the two increases as the temperature is lowered, and the Fermi level is buried more and more in the valence bands. Therefore, this sample is expected to be completely degenerate.

The temperature dependent Hall data taken for this sample is shown in Figure 12. The scattering parameter for this sample in Table 1 shows that this mobility curve was fit with lattice scattering, ionised impurity scattering, and alloy scattering.

It can be seen in Figure 12 that the other two scattering mechanisms are stronger in this sample. However, the main scattering mechanism is still the ionised impurities, and again only the constant term is taking part in the scattering. At low temperatures the ionised impurity scattering is the only one present, and so the mobility levels out. At high temperatures the alloy scattering term and the lattice scattering term start to affect the mobility, and cause it to drop off.

4. $GaAs_{0.5}Sb_{0.5}$

This sample is an alloy: it is approximately half GaAs and half GaSb. It has not been intentionally doped, but has a measured average bulk concentration of holes of 2.45×10^{16} cm^{-3}. There are no acceptor radius densities for this sample, as it is undoped. However, it is expected that the sample will be non-degenerate, since there are no acceptor levels for the holes to travel in. This is not completely confirmed by the location of the Fermi energy. The Fermi level is right at the edge of the valence band for 4 K. At 20 K, the Fermi level is $2k_BT$ above the valence band, and at 90 K the Fermi level is $4k_BT$ above the valence band.

The temperature dependent Hall data taken for this sample is shown in Figure 13. The scattering parameter for this sample in Table 1 shows that this mobility curve was fit with lattice scattering, ionised impurity scattering, and alloy scattering.

It can be seen in Figure 13 that all three scattering mechanisms are important in this sample. At low temperatures, the ionised impurity scattering is strongest. This time though, because this is not a degenerate semiconductor, there is no constant term in the ionised impurity scattering formula. The mobility of the sample goes to zero at low temperatures, in accordance with only the exponential term taking part in the scattering. This is seen also in the fit values in Table 1, as the value for the constant is zero. At moderate temperatures, the alloy scattering term takes over

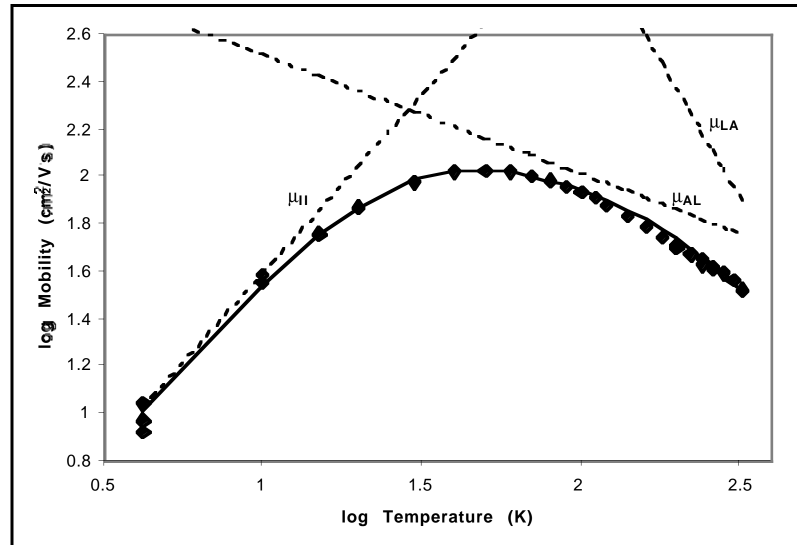

Figure 13: The temperature dependent Hall data for $GaAs_{0.5}Sb_{0.5}$. The dashed lines are the individual mobilities, while the solid line is the total fit.

and dominates the mobility. However, at high temperatures, the lattice scattering term starts to take over. This is shown in Figure 13 at the highest temperatures, where the experimental data starts to drop below the alloy scattering mobility curve.

5. $GaAs_{0.462}Sb_{0.538}$

This sample is an alloy: it is approximately half GaAs and half GaSb. It has been moderately doped to an acceptor level of 1.05×10^{18} cm^{-3}, but has a measured average bulk concentration of holes of 1.04×10^{18} cm^{-3}. This doping level gives an effective acceptor radius that is approximately three times larger than the Bohr radius, so it is expected that the sample will be on the border between non-degenerate and degenerate semiconductors. This is suggested also by the location of the Fermi energy at various temperatures. The Fermi level is $10k_BT$ below the valence band for a temperature of 4 K. At 110 K the Fermi level is right at the valence band edge, And, at room temperature, the Fermi energy is $1.5k_BT$ above the valence band.

The temperature dependent Hall data taken for this sample is shown in Figure 14. The scattering parameter for this sample in Table 1 shows that this mobility curve was fit with lattice scattering, ionised impurity scattering, and alloy scattering.

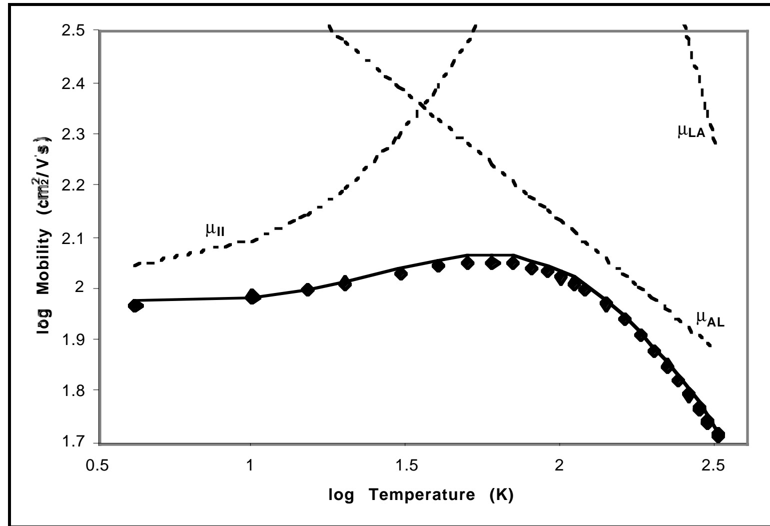

Figure 14: The temperature dependent Hall data for $GaAs_{0.462}Sb_{0.538}$. The dashed lines are the individual mobilities, while the solid line is the total fit.

It can be seen in Figure 14 that two of the three scattering mechanisms are important in this sample. At low temperatures the ionised impurity scattering is strongest, and because this is a partially degenerate semiconductor, the mobility levels off at a nonzero value. This is seen also in the fit values in Table 1, as the value for the constant is nonzero. At moderate temperatures, the alloy scattering term takes over and dominates the mobility, as the ionised impurity term has grown exponentially due to its temperature dependence. At high temperatures, the lattice scattering term starts to show up, but the scattering is still mostly due to alloys. This can be seen in Figure 14 where the experimental data starts to drop away from the alloy scattering mobility curve.

6. GaSb

This sample is a pure GaSb sample (no As) that has been doped to a level of 2.80×10^{19} cm^{-3}. The value for the measured average bulk concentration of holes for this sample, 1.71×10^{20} cm^{-3}, is a factor of 10 larger than the doping level. This doping level gives an effective acceptor radius that is smaller than the Bohr radius. Therefore, this sample is expected to be degenerate. This can be confirmed by calculating the location of the Fermi level, using the bulk concentration of holes and Eq. (5). This calculation shows that the Fermi level is always at least $10k_BT$ below the valence band edge, even at room temperature. Therefore, this sample is expected to be completely degenerate.

The temperature dependent Hall data taken for this sample is shown in Figure 15. The scattering parameter for this sample in Table 1 shows that this mobility curve was fit with lattice scattering, ionised impurity scattering, and space charge scattering. Alloy scattering was not used as this is not an alloy.

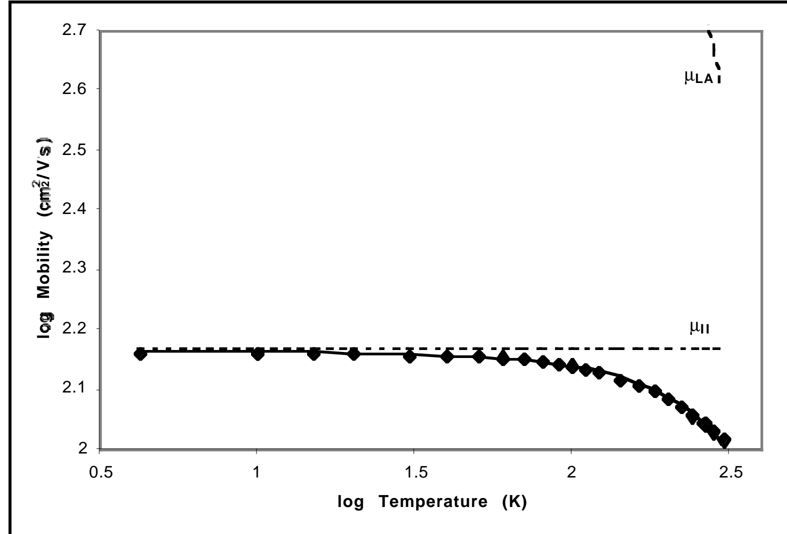

Figure 15: The temperature dependent Hall data for GaSb. The dashed lines are the individual mobilities, while the solid line is the total fit.

The values of the fitting parameters show that the most important scattering mechanism here is the constant term in ionised impurity scattering. This can be seen by the small value of the constant and the zero proportionality factor for ionised impurity scattering dependence on temperature. This fact is also clear from Figure 15, as the ionised impurity mobility curve is perfectly constant, and is just about the only visible mobility curve on the graph. Lattice scattering is weak in this sample, though it does start to have an effect at the highest temperatures where it causes the drop in the experimental mobility. Space charge scattering is almost negligible, as its effect is more than 5 times weaker than that of lattice scattering.

V. Discussion

A. Room Temperature Alloy Scattering

The fit done to the data shown in Figure 8 is a good fit. The total mobility curve almost follows the data, in spite of the rather large variance. The theoretical curve even shows the asymmetrical dependence of the mobility on the Sb content. In the theoretical curve, this asymmetry occurs due to the Sb content dependence of the alloy scattering.

There are two problems with the fit done for this data. The first is that the form that was assumed for the ionised impurity scattering mobility has it as being almost linear as a function of the Sb content. In other papers on this subject,[15] the mobility without alloy scattering taken into account is more bowed in the centre of the graph than this. This inconsistency could mean that the equation used for the ionised impurity scattering is incorrect, but this is unlikely. A more likely situation is that ionised impurity and alloy scattering are not the only scattering mechanisms present in the samples. Attempts should be made to try adding other scattering mechanisms into the fit to try and make it better.

The second problem with this fit is the value of 1.868 eV it gives for the alloy scattering potential. According to the theory for alloy scattering, the alloy scattering potential is supposed to be approximately the valence band offset between the two materials. For $GaAs_{1-x}Sb_x$, this is approximately 1 eV or less. The value obtained here is therefore about twice as large as expected. This could mean that the idea proposed in the theory that the alloy scattering potential is related to the valence band offset is incorrect. A more plausible reason for this factor of two, is that all the scattering mechanisms present

have not been included in the fit. This agrees with the statements made earlier that the fit is not quite right, and could stand to be improved on by using additional scattering mechanisms. By Eq. (21), these additional mechanisms would bring down the mobility, which means that the alloy scattering mobilities can be larger. This corresponds to a smaller alloy scattering potential, which is exactly what is desired here.

B. Temperature Dependent Scattering

Each of the samples was analysed to find its bulk concentration of holes (p), listed in Table 1. These can then be compared with the concentration of acceptor atoms (N_a) that the sample was doped with. Since most of the samples are degenerate, or near to it, the acceptors should all be ionised. This means that the bulk concentration of holes should be approximately equal to the acceptor concentration. This is the case for four of the six samples: GaAs, $GaAs_{0.919}Sb_{0.081}$, $GaAs_{0.535}Sb_{0.465}$, and $GaAs_{0.462}Sb_{0.538}$.

In the undoped sample, $GaAs_{0.5}Sb_{0.5}$, there are no acceptor atoms (ideally), and so the bulk concentration of holes would be expected to be equal to the intrinsic concentration of holes in the sample. However, these intrinsic concentrations are dependent on temperature, so they go to zero at low temperatures, and have a maximum value for this material of about 10^{10} cm^{-3} at room temperature. This is not at all the behaviour of the bulk concentration of holes shown in Figure 9, where the concentration stays fairly constant at values higher than 10^{16} cm^{-3}. This suggests that there are acceptor impurities included in the material unintentionally during the growth process, which are contributing to this increased concentration of holes.

The GaSb sample was doped at a concentration of 2.8×10^{19} cm^{-3}, however the Hall measurements yielded a value for the bulk concentration of holes of 1.71×10^{20} cm^{-3}. This is almost a factor of 10 larger than the expected value for the hole concentration. This could not be due to any kind of intrinsic hole concentration, because it is not temperature dependent and the values are much too large to account for that. It could be due to unintentionally added impurities in the sample, but this is a very large concentration so it seems unlikely. The most plausible reason for this discrepancy is human error.

There were three methods used to determine the degeneracy of the samples. The first was to calculate the Bohr radius of the holes, to see if it was larger than the radius of separation for each acceptor atom. The second was to calculate the location of the Fermi energy in relation to the valence band. The third was to use the plot of mobility as a function of temperature at low temperatures to see if there is carrier freeze-out occurring. Of these three methods, the third is the most reliable and yields the best results. From the third method, it is determined that four of the samples are degenerate: GaAs, $GaAs_{0.919}Sb_{0.081}$, $GaAs_{0.535}Sb_{0.465}$, and GaSb. The $GaAs_{0.462}Sb_{0.538}$ sample was partially degenerate, as it had a peak mobility around 60 K, and then decreased but levelled off at a non-zero mobility. The undoped sample, $GaAs_{0.5}Sb_{0.5}$, was completely non-degenerate, as its mobility went to zero at low temperatures.

The first and second methods are not as reliable as the third method. The first method is not as accurate because there can still be a small amount of transport in the acceptor band, even if the acceptor radius is not strictly less than the Bohr radius. If the first method were used to determine degeneracy, then the GaAs sample would be borderline non-degenerate, and the $GaAs_{0.462}Sb_{0.538}$ sample would be almost completely non-degenerate. The second method is not as reliable because the choice of defining degeneracy as occurring when the Fermi energy is less than $4k_BT$ above the valence band is arbitrary. Strictly speaking, this energy difference should be the location of the acceptor

impurity level in relation to the valence band. However, since this value is rarely known, the arbitrary definition has to be used.

The inclusion of surface charge or deformation potential scattering into the fits done to the two samples that do not have alloy scattering, GaAs and GaSb, would seem to be unnecessary. In both cases, the scattering proportionality constant was so large that the mobilities had almost no effect on the overall mobility. For surface charge scattering, it can be assumed that this mechanism will therefore not have an effect on the alloys. However, the deformation potential scattering is expected to be dependent the strain in alloys, and so should have almost no effect in non-alloys. It can therefore not be assumed to be negligent in the alloy scattering.

The use of a constant in the ionised impurity scattering, as described in Eq. (34), did not have the desired effect in most of the samples. In the heavily doped samples that were expected to be degenerate, the temperature dependent term in the scattering was set to zero in the fitting process. This left only the constant term to determine the mobility at low temperatures. In the undoped non-degenerate sample, $GaAs_{0.5}Sb_{0.5}$, the constant was set to zero by the fitting process. That left only the exponential temperature dependence term to determine the low temperature mobilities. The only sample where the fitting process used both the constant and the exponential temperature dependence terms was in the moderately doped $GaAs_{0.462}Sb_{0.438}$. This sample was borderline between being degenerately doped and being non-degenerate, which can be seen in the mobilities of Figure 14. The mobility peaks at about 60 K and then starts to decrease, as in the undoped case. However, the mobility eventually levels out at a nonzero value. The only way to fit this to the scattering mechanisms presented here is to use an equation similar to Eq. (34). If the ionised impurity scattering is included, it will cause the mobility to drop to zero. If the constant is used, it will not be possible to get the peak that is so evident in Figure 14. The theoretical mobility must be something that increases with temperature, but is nonzero at low temperatures.

The alloy scattering potentials obtained from the fits, and listed in Table 1 for each sample, all seem to agree very nicely with each other. All four of them are in the range of 1.3 eV to 1.6 eV. The value obtained from the room temperature mobilities of the undoped samples, 1.868 eV, is also close to these values. These values are not quite as expected from the theoretically predicted value of 1.0 eV or less, however they are reasonably close to this prediction. As mentioned previously, one reason for the discrepancies might be that not all the scattering mechanisms present in the sample have been included in the theory. In particular, deformation potential scattering might possibly be important here, as it is strong in alloys. Also, since it has the same temperature dependence as alloy scattering, then adding it into the fit would not affect the graph of the mobility, but would affect the fit parameters. Thus, adding in deformation potential scattering would cause the alloy scattering potential to decrease accordingly. These values should then be closer to the expected value. Also, it will not affect the quality of the fit, which is important since all of the fits are good.

VI. Conclusions

The scattering mechanisms in the $GaAs_{1-x}Sb_x$ system have been examined to determine the mechanisms present, and their relative strengths. Also, the degeneracy condition on heavily doped materials in this system has been investigated.

Mobility data has been analysed for some undoped samples raging in Sb content from GaAs to GaSb. Two scattering mechanisms that were determined to be present are ionised impurity scattering and alloy scattering. Ionised impurity scattering shows an

almost linear dependence on the Sb content of the sample, however alloy scattering shows a strong dependence on the Sb content. The alloy scattering potential was found to be 1.868 eV for this data.

Six samples have also been examined at temperatures ranging from 4.2 K to 320 K. These samples ranged in content from GaAs to GaSb, and in doping from undoped to heavily doped. Four of the samples were found to be degenerately doped, one was found to be borderline, and one was found to be non-degenerate. The degenerate samples levelled off at low temperatures to their highest mobility. It was found that all of them had a type of ionised impurity scattering that does not depend on temperature. They also all had lattice scattering to various degrees. The samples that were alloys also had their mobilities lowered by alloy scattering. The non-degenerate sample was found to have ionised impurity scattering, lattice scattering, and alloy scattering. Unlike the degenerate samples though, the ionised impurity scattering in this sample was temperature dependent, and caused the mobility to drop to zero at low temperatures. The borderline sample was found also to have alloy scattering, lattice scattering, and ionised impurity scattering. In this case, however, the mobility peaked as in the non-degenerate case, but then descended and levelled off at a nonzero value as in the degenerate case. This meant that a combination of the two types of ionised impurity scattering had to be used to fit the data properly.

An alloy scattering potential was determined for the undoped room temperature mobilities, and also for each of the alloy samples investigated at varying temperatures. The potentials were found to range from 1.3 to 1.8 eV. These values are 1.5 to 2.0 times larger than the maximum expected alloy scattering potential from the theory. This discrepancy probably occurred because not all of the scattering mechanisms were considered here.

One likely candidate for a scattering mechanism that could explain these discrepancies is deformation potential scattering. It has the same temperature dependence as alloy scattering, and so would not affect the good fits for the mobilities that vary with temperature. However, it has a different content (x) dependence than alloy scattering, and so would hopefully improve the fit in the case of the room temperature mobilities. For both, it would cause a reduction in the alloy scattering potentials, which would bring them closer to the expected value.

VII. Acknowledgements

I would like to thank Dr. Simon Watkins for his time spent on this project, and also for his help in explaining what was going on. I would also like to thank Patella for his help with the apparatus and taking the measurements.

VIII. References

[1] Jinsheng Hu, "*MOCVD Growth and Optical properties of GaAsSb/InGaAs and GaAsSb/InP Heterostructures*," PhD Thesis, Simon Fraser University, 1999.

[2] X. G. Xu, J. Hu, S. P. Watkins, N. Matine, M. W. Dvorak, and C. R. Bolognesi, "*Metalorganic vapor phase epitaxy of high-quality $GaAs_{0.5}Sb_{0.5}$ and its application to heterostructure bipolar transistors*," Applied Physics Letters, Vol. 74, No. 7, February 1999, p 976-978.

[3] Charles Kittel, "*Introduction to Solid State Physics*," 7th Ed., (John Wiley & Sons, Inc.: Toronto, Canada, 1996), p 210.

[4] Charles M. Wolfe, Nick Holonyak Jr., Gregory E. Stillman, "*Physical Properties of Semiconductors*," (Prentice-Hall, Inc.: Englewood Cliffs, New Jersey, 1989), p 86.

[5] Ben G. Streetman, "*Solid State Electronic Devices*," 4th Ed., (Prentice-Hall, Inc.: Upper Saddle River, New Jersey, 1995), p 440-442.

[6] Stillman, p 125-127.

[7] Stillman, p 343-347.

[8] L. J. van der Pauw, "*A Method of Measuring Specific Resistivity and Hall Effect of Discs of Arbitrary Shape*," Philips Research Reports, Vol. 13, No. 1, February 1958, p 1-9.

[9] J. W. Harrison and J. R. Hauser, "*Alloy scattering in ternary III-V compounds*," Physical Review B, Vol. 13, No. 12, June 1976, p 5347-5350.

[10] Streetman, p 87.

[11] J. S. Blakemore, Journal of Applied Physics, Vol. 53, No. 10, October 1982, p R123-R181.

[12] K. B. Joelson, Y. Fu, W.-X. Ni, and G. V. Hansson, "*Hall factor and drift mobility for hole transport in strained* $Si_{1-x}Ge_x$ *alloys*," Journal of Applied Physics, Vol. 81, No. 3, February 1997, p 1264-1269.

[13] M. Lannoo, J. Bourgoin, "*Point Defects in Semiconductors*," Vol. 2, (Springer-Verlar: New York, New York, 1981).

[14] Herbert S. Bennett, "*Majority and minority electron and hole mobilities in heavily doped gallium aluminum arsenide*," Journal of Applied Physics, Vol. 80, No. 7, October 1996, p 3844-3853.

[15] D. C. Look, D. K. Lorance, J. R. Sizelove, C. E. Stutz, K. R. Evans, and D. W. Whitson, "*Alloy scattering in p-type* $Al_xGa_{1-x}As$," Journal of Applied Physics, Vol. 71, No. 1, January 1992, p 260-266.